


***In situ* characterization of qubit-drive phase distortions**M.F. Gely<sup>✉,\*†</sup>, J.M.A. Litarowicz,<sup>†</sup> A.D. Leu<sup>✉</sup>, and D.M. Lucas*Department of Physics, Clarendon Laboratory, University of Oxford, Parks Road, Oxford, OX1 3PU, United Kingdom* (Received 6 November 2023; revised 2 May 2024; accepted 2 July 2024; published 1 August 2024)

Reducing errors in quantum gates is critical to the development of quantum computers. To do so, any distortions in the control signals should be identified; however, conventional tools are not always applicable when part of the system is under high vacuum, cryogenic, or microscopic. Here, we demonstrate a method to detect and compensate for amplitude-dependent phase changes, using the qubit itself as a probe. The technique is implemented using a microwave-driven trapped-ion qubit, where correcting phase distortions leads to a threefold improvement in the error of single-qubit gates implemented with pulses of different amplitudes, to attain state-of-the-art performance benchmarked at  $1.6(4) \times 10^{-6}$  error per Clifford gate.

DOI: [10.1103/PhysRevApplied.22.024001](https://doi.org/10.1103/PhysRevApplied.22.024001)**I. INTRODUCTION**

High-fidelity control of quantum systems is crucial to quantum computing, as it can drastically minimize the overhead associated with error correction [1]. In many platforms, quantum gates are driven by laser, radio-frequency, or microwave pulses, where low error rates depend on the accurate control of signal amplitude and phase. Distortions induced by the chain of components generating and delivering this drive signal should therefore be identified and corrected. A common compensation technique is to use “predistortion,” such that distortions produce the desired pulse [2]. This is used in NMR [3], EPR [4], Rydberg atoms [5], Bose-Einstein condensates [6], and superconducting circuits [7–9]. In trapped ions [10], predistortion has been used to compensate for thermal transients in microwave circuitry [11] or for compensating filtering in fast shuttling operations [12]. Successful predistortion relies, however, on an accurate model of the drive chain, part of which is, for trapped ions, under high vacuum, microscopic, and possibly cooled cryogenically [13]. The use of conventional tools such as network analyzers is therefore not always possible.

Here, we demonstrate how a trapped-ion qubit can be used as a sensor to characterize the distortion of gate pulses [7–9,14]. This complements other techniques relying on

atomic systems, such as Bose-Einstein condensates [15] or ultracold atoms [16], to image near-field microwaves. Specifically, we present a scheme that coherently amplifies the amplitude-dependent phase change of a microwave field. Predistortion is shown to compensate for this drive-chain imperfection, leading to a threefold reduction in single-qubit gate error when gates are implemented with pulses of different amplitudes, to attain state-of-the-art performance benchmarked at  $1.6(4) \times 10^{-6}$  error per Clifford gate.

**II. APPARATUS AND EXPERIMENTAL OBSERVATIONS**

Experiments are carried out using a trapped-ion qubit driven by near-field microwaves [11,17–22]. Our qubit is defined by the hyperfine levels  $|0\rangle = |F = 3, M_F = 1\rangle$  and  $|1\rangle = |F = 4, M_F = 1\rangle$  of the ground-state manifold  $4S_{1/2}$  of  $^{43}\text{Ca}^+$ , which form a clock transition at our static magnetic field strength of 28.8 mT. The ion is trapped 40  $\mu\text{m}$  above a surface “chip” trap, which features a microwave (MW) electrode used to drive the magnetic dipole moment of the qubit. Amplitude-shaped pulses at 123 MHz are generated using an arbitrary waveform generator (AWG), then up-converted using a 3-GHz source and an IQ mixer to be brought into on resonance with the qubit frequency at 3.1 GHz. After amplification to approximately 400 mW, the microwaves are delivered into the vacuum chamber to the surface trap, where they drive the qubit. A simplified schematic of the experimental setup is shown in Fig. 1(a), with more detail in Sec. S2 of the Supplemental Material [23]. Details on the trap and qubit state preparation and readout can be found in Ref. [24].

\*Contact author: [mario.f.gely@gmail.com](mailto:mario.f.gely@gmail.com)

†These two authors contributed equally to this work.

*Published by the American Physical Society under the terms of the [Creative Commons Attribution 4.0 International](https://creativecommons.org/licenses/by/4.0/) license. Further distribution of this work must maintain attribution to the author(s) and the published article’s title, journal citation, and DOI.*

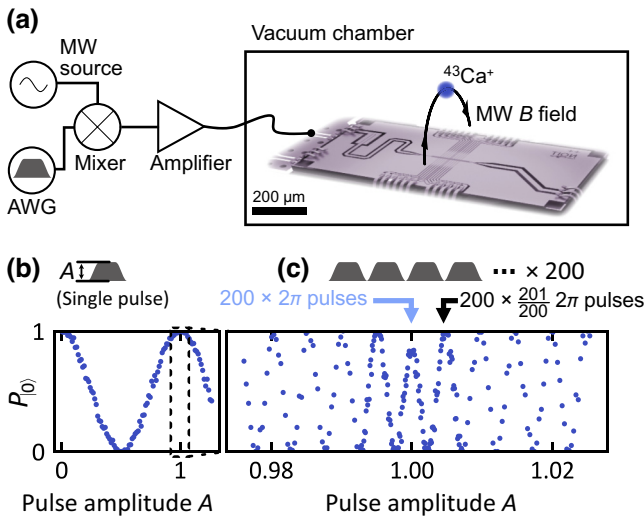


FIG. 1. The nonlinear drive-chain and Rabi-oscillation distortion. (a) An overview of the experimental setup, showing a simplified schematic of the MW drive chain delivering pulses to a  $^{43}\text{Ca}^+$  trapped-ion qubit. The potential nonlinearity of the MW components needs to be identified and compensated for. The ion height and MW field are not to scale. (b) Delivering a single pulse of fixed duration but varied amplitude  $A$  enables the observation of Rabi oscillations. Here,  $P_{|0\rangle}$  corresponds to the probability of measuring the initial state  $|0\rangle$  after the pulse. The amplitude is normalized such that  $A = 1$  corresponds to a pulse driving a  $2\pi$  rotation of the qubit. (c) When  $N$  pulses are delivered, the initial qubit state is in principle recovered when the pulse amplitude is an integer multiple of  $1/N$ . Here, this is verified for  $N = 200$  and, surprisingly, is not the case for  $A = 1$ . This exceptional point corresponds to the case in which  $N \times 2\pi$  pulses are nominally delivered. As explained in Fig. 2, this is a signature of a phase-amplitude relation, stemming from the nonlinearity of MW components.

These MW pulses, resonant with the qubit transition, will drive Rabi oscillations, as shown in Fig. 1(b). Given the 1-ns timing resolution of our control system and our pulse duration of 1.2  $\mu\text{s}$ , varying the pulse amplitude at the AWG (with 15-bit resolution) offers a more precise method of tuning the pulse area than varying the pulse duration ( $3 \times 10^{-5}$  precision rather than  $8 \times 10^{-4}$ ). We therefore vary the pulse amplitude rather than the more usual pulse time in these measurements but scanning the pulse duration would produce a similar effect in Figs. 1(b) and 1(c). For a fixed pulse shape and duration, we define a pulse-amplitude scaling factor  $A$  such that  $A = 1$  produces a  $2\pi$  rotation of the qubit. When  $A$  is swept from 0 to 1, the probability  $P_{|0\rangle}$  of recovering the initial qubit state  $|0\rangle$  will undergo a single oscillation as shown in Fig. 1(a). When driving the qubit with a train of  $N$  (identical) pulses rather than one pulse,  $P_{|0\rangle}$  should undergo  $N$  oscillations rather than one in the same amplitude span. Indeed, at a pulse amplitude  $A = n/N$ , if  $n$  is an integer, the cumulative effect of the pulse train should be to induce  $n$  full rotations

of the qubit state around the Bloch sphere. The resulting recovery to the initial state is observed in the measurement of Fig. 1(c), except for the case  $A = 1$ , nominally corresponding to a train of  $2\pi$  rotations.

### III. THEORETICAL DESCRIPTION OF THE PHENOMENON

To explain this phenomenon, we consider a change in MW phase  $\phi(t)$  during the pulse, proportional to the pulse amplitude  $a(t)$ . We normalize  $a$  such that  $a(t) = A$  during the “plateau” of the pulse. The phase variation is assumed to be characterized by the phase-amplitude proportionality factor  $\phi' = \partial\phi/\partial a$ , such that we have  $\phi(t) = \phi'a(t) + \phi_0$ . Such a phase-amplitude relation would come into play while ramping up or down the pulse, which is done in this experiment over a duration of  $t_{\text{ramp}} = 200$  ns per ramp (400-ns total ramping time over a pulse). This consideration is motivated by the number of potentially nonlinear elements in the MW drive chain (the AWG, the mixer, and the amplifier). Without loss of generality, we set  $\phi(t) = 0$  during the “plateau” of the pulse such that the small phase variation perturbs the pulse—during the ramping—away from the ideal  $x$  rotation. The resulting physics can be understood by constructing an equivalent unitary to that driven by the pulse train, where phase deviations manifest as small  $y$  rotations at the beginning and end of each pulse train. This is schematically shown in Fig. 2(b) and formally derived in Sec. S1A of the Supplemental Material [23].

These small  $y$  rotations will nearly always be inconsequential, as the dominant  $x$  rotation will dynamically decouple the qubit from noncommuting  $y$  rotations. However, this is not the case at the exceptional  $A = 1$  point in Fig. 1(c), where the  $x$  rotation is an identity operation, which then commutes with  $y$  rotations. Indeed, at  $A = 1$ , each pulse is approximately a  $2\pi$  rotation around the  $x$  axis and ramping up or down the pulse always occurs when the qubit state is in the same area of the Bloch sphere. The  $y$  rotations will then coherently add up such that, after  $N = 200$  pulses, the total  $y$  rotation produces a noticeable decrease in  $P_{|0\rangle}$ . This is schematically shown in Fig. 2(c), with inflated ramping durations and phase variations such that the effect is noticeable after a few pulses. When pulses do not produce a  $2\pi$  rotation, ramping up or down will occur at varying areas of the Bloch sphere as the train of pulses progresses and the  $y$  rotations tend to average out. This is illustrated in the case of  $2\pi/3$  pulses in Fig. 2(d). As derived in Sec. S1B of the Supplemental Material [23], in the former case, phase variations have an impact on  $P_{|0\rangle}$  of order  $\sim(N\phi')^2$ , whereas in the latter, the effect is much smaller, of order  $(N\phi')^4$ .

### IV. EXPERIMENTAL VERIFICATION

To verify this interpretation, we add a compensation phase proportional to the pulse amplitude  $\phi_c(t) = a(t)\phi'_c$

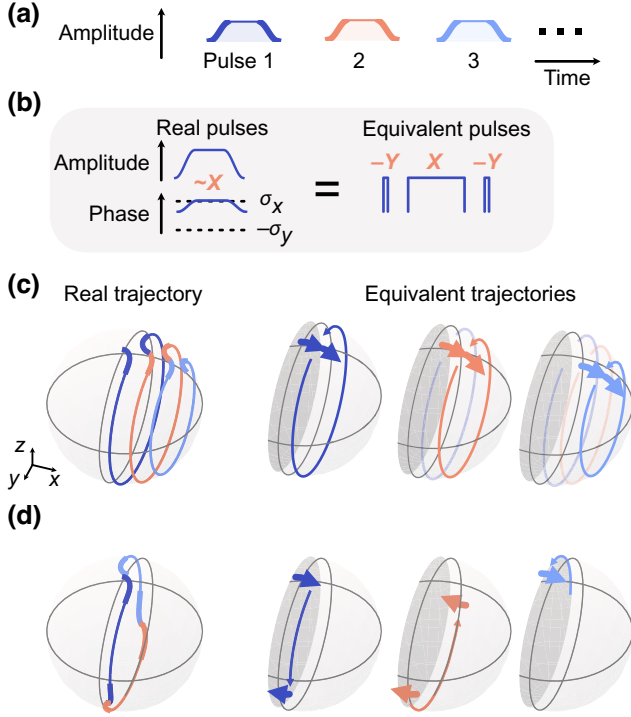


FIG. 2. The coherent amplification of phase variations. (a) A schematic of the train of pulses applied to the qubit. These are intended to produce  $x$  rotations. (b) If the MW phase depends on amplitude (“real pulses”), the resulting deviations in phase during ramp-up or -down can be described by a small  $y$  rotation (“equivalent pulses”). (c),(d) The trajectory driven on the Bloch sphere by three successive pulses for the real and equivalent pulses. The ramping or resulting  $y$  rotations are shown in bold or with a thicker arrow. (c) In the case of a train of  $2\pi$  pulses, since the qubit returns to the same part of the Bloch sphere for ramp-up or -down of the pulse amplitude, the small  $y$  rotations add up coherently, producing the exceptional  $A = 1$  point in Fig. 1(c). (d) Otherwise—e.g., here with  $2\pi/3$  pulses—ramp-up or -down occurs on varying parts of the Bloch sphere, such that the  $y$  rotations cancel out, ensuring a return to the initial qubit state. To make the effect visible for just three pulses, ramp durations and phase deviations are exaggerated with respect to the experiment.

in the pulses generated by our AWG. This “predistorted” MW pulse then has a phase given by

$$\phi(t) = \phi_n(t) + \phi_c(t) = a(t)(\phi'_n + \phi'_c) + \phi_0, \quad (1)$$

where  $\phi_n$  designates the phase variation native to the drive chain. While varying the parameter  $\phi'_c$ , we measure the distorted Rabi oscillations to show that full contrast at  $A = 1$  can be recovered for  $\phi'_c = -2\pi \times 1.8 \times 10^{-3}$  radians (Fig. 3). Here, we are again using a train of 200 pulses, just as in Fig. 1(c). This indicates that the phase does indeed change (linearly) with the MW amplitude. A control experiment providing further confirmation of this fact is presented in Sec. S2 of the Supplemental Material [23].

Scanning both the pulse amplitude  $A$  and the phase compensation  $\phi'_c$  while monitoring  $P_{|0\rangle}$  reveals a symmetry in their influence [Fig. 3(b)]. Indeed, while deviations of the pulse amplitude away from  $A = 1$  increase the amount of net rotation around the  $x$  axis, increased phase variation during pulse ramping increases the accumulated  $y$  rotation over the train of pulses. While a horizontal line cut of Fig. 3 [Fig. 3(e)] describes Rabi oscillations induced by  $x$  rotations, a vertical line cut [Fig. 3(a)] describes Rabi oscillations induced by  $y$  rotations. This is demonstrated more formally in Sec. S1B of the Supplemental Material [23] using perturbation theory, showing that for  $|A - 1|, |\phi(t)| \ll 1$ , a train of  $N$  pulses drives the unitary evolution

$$\hat{U} = \exp(iN\Omega_x\hat{\sigma}_x + iN\Omega_y\hat{\sigma}_y), \quad (2)$$

where  $\Omega_x \propto (A - 1)$  and  $\Omega_y \propto \phi'$ . This unitary results in the ring pattern observed in the measurement of Fig. 3(b):

$$P_{|0\rangle} = \frac{1}{2} \left( 1 + \cos \left( N \sqrt{\Omega_x^2 + \Omega_y^2} \right) \right). \quad (3)$$

## V. APPLICATION TO SINGLE-QUBIT GATES

While the phase change over a noncompensated pulse is small, it can be a leading source of error in the high-fidelity logic operations on trapped-ion qubits. Scanning the compensation parameter while monitoring  $P_{|0\rangle}$  [Fig. 3(a)] constitutes a rapid calibration procedure sufficient to mitigate phase variations. To demonstrate this, we scan the phase-compensation parameter  $\phi'_c$  while monitoring the single-qubit Clifford gate error with randomized benchmarking [25] [Fig. 4(a)]. The error is reduced from  $5(2) \times 10^{-6}$  to  $1.6(4) \times 10^{-6}$  when using the phase compensation identified in Fig. 3(a). In this case, identifying and compensating for this small variation in phase brings single-qubit gate performance to state-of-the-art error rates [19,22]. The sensitivity the technique, considering the presence of decoherence, drifts, or state-preparation-and-measurement errors, is discussed in Sec. S1D of the Supplemental Material [23]. This calibration routine could be extended to more complex phase-amplitude relations  $\phi(t) = \phi_0 + \phi'a(t) + \phi''a(t)^2 + \phi'''a(t)^3 + \dots$  by maximizing  $P_{|0\rangle}$  as in Fig. 3(a) as a function of  $\phi'$ , but also higher-order phase-compensation parameters  $\phi''$  and  $\phi'''$ .

We note that this problem is not present in previously reported error budgets [22] due to the different decomposition of Clifford gates into native MW pulses. Here, we decompose Clifford gates into  $\pi$  and  $\pi/2$  pulses of the same duration and the bulk of the error arises due to the  $\times 2$  variation in pulse amplitude, which produces a change in the relative phases of  $\pi$  and  $\pi/2$  pulses. This error can thus also be mitigated by decomposing Clifford gates into only  $\pi/2$  pulses, at the expense of increasing the average number of pulses per Clifford from approximately 1 to

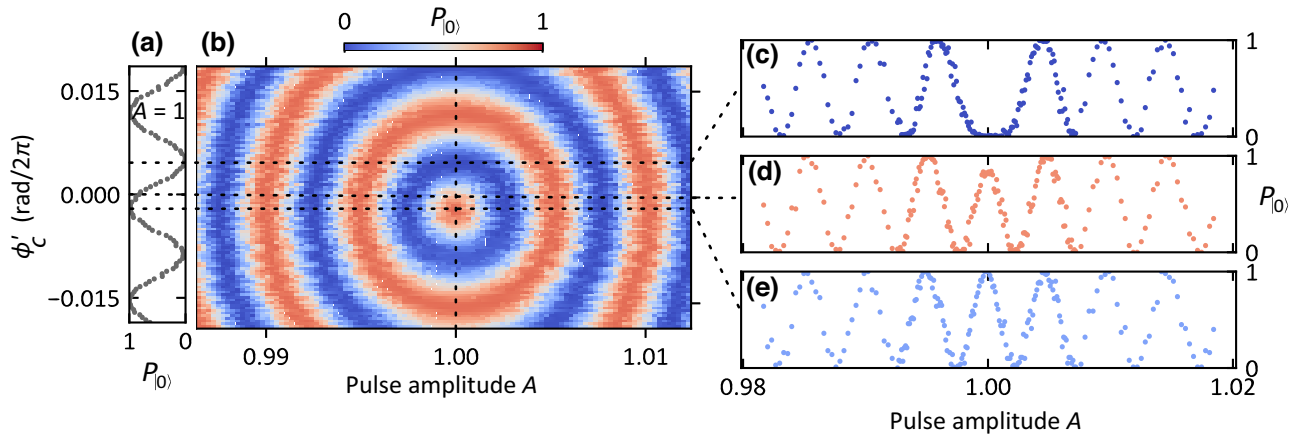


FIG. 3. MW-phase predistortion. Rabi oscillations are measured as in Fig. 1(c) for a train of  $N = 200$  pulses. (a) For  $A = 1$ , we vary the proportionality factor between phase and amplitude  $\phi'_c$ , implemented in our AWG, while monitoring  $P_{|0\rangle}$ . Compensation of the effect is obtained for  $\phi'_c = -2\pi \times 1.8 \times 10^{-3}$  radians. (b)  $P_{|0\rangle}$  as a function of both  $\phi'_c$  and pulse amplitude  $A$ , where selected transects show that the effect can be accentuated [(c),  $\phi'_c = 2\pi \times 4.9 \times 10^{-3}$ ] with respect to the case where the phase is not intentionally varied [(d),  $\phi'_c = 0$ ], or compensated for (e).

approximately 2.2. Since the pulse time is dominated by the interpulse delay imposed by our control system, this increases the effective gate time and the impact of decoherence. This option has been utilized in Ref. [22], leading to similar gate errors. The residual error from phase variation during pulse ramping is then negligible. Alternatively,  $\pi$  pulses can be implemented with twice the duration of  $\pi/2$  pulses, with the pulse area fine tuned through the pulse

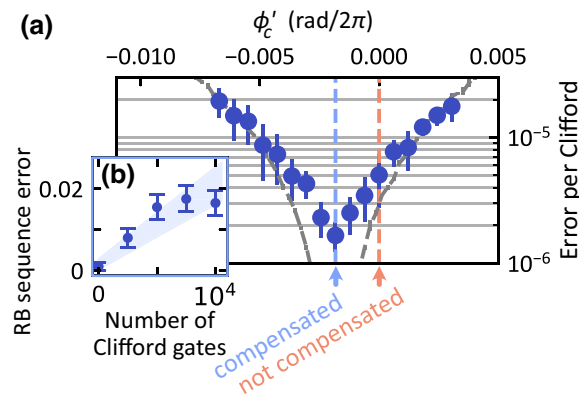


FIG. 4. The application to high-fidelity quantum gates. (a) The dots are single-qubit gate errors measured using randomized benchmarking (RB) as a function of the phase compensation. The error is reduced from  $5(2) \times 10^{-6}$  to  $1.6(4) \times 10^{-6}$  when using the phase compensation identified in Fig. 3(a). The error scaling at higher phase-compensation values is consistent with simulated RB data (gray dashed lines). Lower errors are limited by other physical mechanisms [22]. (b) The RB sequence error as a function of the number of Clifford gates per sequence. This corresponds to lowest error where the phase variations are compensated for. The gate error is on par with state-of-the-art errors across all quantum computing platforms [19,22].

amplitude, minimizing the impact of phase variations, and the average duration of a Clifford gate. A calibration of phase variations is also useful in more complex composite pulse schemes; in particular, when we want to leverage the fine pulse-amplitude control from pulse to pulse—e.g., in the ion-addressing scheme of Ref. [22]. In the addressing experiment, the combination of weak pulses (at least half the amplitude used in this work) and the dominance of drift-induced errors makes the impact of phase variations negligible. The average error over 100 different addressing pulse sequences is theoretically  $9.0(2) \times 10^{-7}$ , much smaller than the average error measured at  $3.4 \times 10^{-5}$ . However, by simply doubling the amplitude and  $\phi'_n$ , the error would have been considerable, at  $1.5(5) \times 10^{-5}$  per gate.

By measuring a scattering parameter ( $S_{21}$ ) of the nonlinear components of our MW drive chain, we attempt to understand the native phase variation characterized by  $\phi'_n = 2\pi \times 1.8 \times 10^{-3}$  rad. Unfortunately, such measurements are limited to the phase precision of our vector network analyzer, of approximately  $2\pi \times 10^{-4}$  rad. The only component showing measurable phase variation is the amplifier, with  $\phi' = 2\pi \times 0.8 \times 10^{-3}$  (see the measurement details in Sec. S2 of the Supplemental Material [23]). In this experimental context, the Rabi-oscillation distortion is thus a much more sensitive method for diagnostics and compensation. Finally, we note that the measurement scheme of Fig. 1(c) also enables the characterization of other drive-chain distortions. If the Rabi frequency scales linearly with the MW amplitude programmed in the AWG, then the period of oscillations in Fig. 1(c) should remain constant as the amplitude increases. In practice, we find that this is not the case and this measurement constitutes a rapid calibration of this field-amplitude nonlinearity that

could be useful for, e.g., the addressing scheme of Ref. [22], which relies on pulses of varying amplitudes.

## VI. CONCLUSIONS

In conclusion, we have presented a scheme to rapidly identify, and to compensate for, phase-amplitude relations in qubit drives. These phase variations are shown to be a dominant error in our implementation of microwave-driven quantum logic. Predistortion of the phase evolution during the pulse ramping is shown to be an effective mitigation technique. The resulting error rate, measured through randomized benchmarking ( $1.6(4) \times 10^{-6}$  per Clifford gate), is consistent with the state of the art across all quantum computing platforms [19,22]. The scheme is applicable to any qubit system driven by an amplitude-shaped pulse. Since the qubit itself is used to probe the field, it is particularly suited to systems that are partially inaccessible by more conventional sensors; systems that are under vacuum, cryogenic, or micrometer or nanometer in size. For example, the technique could readily be applied to spin qubits, where single-qubit gates are also implemented using gigahertz-frequency-shaped pulses, resonantly driving the qubit transition [26].

## ACKNOWLEDGMENTS

This work was supported by the U.S. Army Research Office (Grant No. W911NF-18-1-0340) and the U.K. Engineering and Physical Sciences Research Council (EPSRC) Quantum Computing and Simulation Hub. M.F.G. acknowledges support from the Netherlands Organization for Scientific Research (NWO) through a Rubicon Grant. A.D.L. acknowledges support from Oxford Ionics Ltd.

- 
- [1] E. Knill, Quantum computing, *Nature* **463**, 441 (2010).
- [2] I. N. Hincks, C. E. Granade, T. W. Borneman, and D. G. Cory, Controlling quantum devices with nonlinear hardware, *Phys. Rev. Appl.* **4**, 024012 (2015).
- [3] Y. Tabuchi, M. Negoro, K. Takeda, and M. Kitagawa, Total compensation of pulse transients inside a resonator, *J. Magn. Reson.* **204**, 327 (2010).
- [4] P. E. Spindler, P. Schöps, W. Kallies, S. J. Glaser, and T. F. Prisner, Perspectives of shaped pulses for EPR spectroscopy, *J. Magn. Reson.* **280**, 30 (2017), Special Issue on Methodological advances in EPR spectroscopy and imaging.
- [5] J. Singh, R. Zeier, T. Calarco, and F. Motzoi, Compensating for nonlinear distortions in controlled quantum systems, *Phys. Rev. Appl.* **19**, 064067 (2023).
- [6] G. Jaeger and U. Hohenester, Optimal quantum control of Bose-Einstein condensates in magnetic microtraps: Consideration of filter effects, *Phys. Rev. A* **88**, 035601 (2013).
- [7] S. Gustavsson, O. Zwiernik, J. Bylander, F. Yan, F. Yoshihara, Y. Nakamura, T. P. Orlando, and W. D. Oliver, Improving quantum gate fidelities by using a qubit to measure microwave pulse distortions, *Phys. Rev. Lett.* **110**, 040502 (2013).
- [8] M. Jerger, A. Kulikov, Z. Vasselin, and A. Fedorov, *In situ* characterization of qubit control lines: A qubit as a vector network analyzer, *Phys. Rev. Lett.* **123**, 150501 (2019).
- [9] S. Lazăr, Q. Ficheux, J. Herrmann, A. Remm, N. Lacroix, C. Hellings, F. Swiadek, D. C. Zanuz, G. J. Norris, M. B. Panah, A. Flasby, M. Kerschbaum, J.-C. Besse, C. Eichler, and A. Wallraff, Calibration of drive nonlinearity for arbitrary-angle single-qubit gates using error amplification, *Phys. Rev. Appl.* **20**, 024036 (2023).
- [10] C. D. Bruzewicz, J. Chiaverini, R. McConnell, and J. M. Sage, Trapped-ion quantum computing: Progress and challenges, *Appl. Phys. Rev.* **6**, 021314 (2019).
- [11] T. P. Harty, M. A. Sepiol, D. T. C. Allcock, C. J. Ballance, J. E. Tarlton, and D. M. Lucas, High-fidelity trapped-ion quantum logic using near-field microwaves, *Phys. Rev. Lett.* **117**, 140501 (2016).
- [12] R. Bowler, U. Warring, J. W. Britton, B. C. Sawyer, and J. Amini, Arbitrary waveform generator for quantum information processing with trapped ions, *Rev. Sci. Instrum.* **84**, 033108 (2013).
- [13] M. E. Poitzsch, J. C. Bergquist, W. M. Itano, and D. J. Wineland, Cryogenic linear ion trap for accurate spectroscopy, *Rev. Sci. Instrum.* **67**, 129 (1996).
- [14] M. Kristen, A. Schneider, A. Stehli, T. Wolz, S. Danilin, H. S. Ku, J. Long, X. Wu, R. Lake, D. P. Pappas, *et al.*, Amplitude and frequency sensing of microwave fields with a superconducting transmon qubit, *npj Quantum Inf.* **6**, 57 (2020).
- [15] C. F. Ockeloen, R. Schmied, M. F. Riedel, and P. Treutlein, Quantum metrology with a scanning probe atom interferometer, *Phys. Rev. Lett.* **111**, 143001 (2013).
- [16] P. Bohi, M. F. Riedel, T. W. Hansch, and P. Treutlein, Imaging of microwave fields using ultracold atoms, *Appl. Phys. Lett.* **97**, 051101 (2010).
- [17] C. Ospelkaus, C. E. Langer, J. M. Amini, K. R. Brown, D. Leibfried, and D. J. Wineland, Trapped-ion quantum logic gates based on oscillating magnetic fields, *Phys. Rev. Lett.* **101**, 090502 (2008).
- [18] U. Warring, C. Ospelkaus, Y. Colombe, K. R. Brown, J. M. Amini, M. Carsjens, D. Leibfried, and D. J. Wineland, Techniques for microwave near-field quantum control of trapped ions, *Phys. Rev. A* **87**, 013437 (2013).
- [19] T. P. Harty, D. T. C. Allcock, C. J. Ballance, L. Guidoni, H. A. Janacek, N. M. Linke, D. N. Stacey, and D. M. Lucas, High-fidelity preparation, gates, memory, and readout of a trapped-ion quantum bit, *Phys. Rev. Lett.* **113**, 220501 (2014).
- [20] G. Zarantonello, H. Hahn, J. Morgner, M. Schulte, A. Bautista-Salvador, R. F. Werner, K. Hammerer, and C. Ospelkaus, Robust and resource-efficient microwave near-field entangling  ${}^9\text{Be}^+$  gate, *Phys. Rev. Lett.* **123**, 260503 (2019).
- [21] R. Srinivas, S. C. Burd, H. M. Knaack, R. T. Sutherland, A. Kwiatkowski, S. Glancy, E. Knill, D. J. Wineland, D. Leibfried, A. C. Wilson, D. T. C. Allcock, and

- D. H. Slichter, High-fidelity laser-free universal control of trapped ion qubits, *Nature* **597**, 209 (2021).
- [22] A. D. Leu, M. F. Gely, M. A. Weber, M. C. Smith, D. P. Nadlinger, and D. M. Lucas, Fast, high-fidelity addressed single-qubit gates using efficient composite pulse sequences, *Phys. Rev. Lett.* **131**, 120601 (2023).
- [23] See the Supplemental Material at <http://link.aps.org/supplemental/10.1103/PhysRevApplied.22.024001> for detailed theoretical derivations and supporting measurements.
- [24] M. A. Weber, C. Löschnauer, J. Wolf, M. F. Gely, R. K. Hanley, J. F. Goodwin, C. J. Ballance, T. P. Harty, and D. M. Lucas, Cryogenic ion trap system for high-fidelity near-field microwave-driven quantum logic, *Quantum Sci. Technol.* **9**, 015007 (2024).
- [25] E. Knill, D. Leibfried, R. Reichle, J. Britton, R. B. Blakestad, J. D. Jost, C. Langer, R. Ozeri, S. Seidelin, and D. J. Wineland, Randomized benchmarking of quantum gates, *Phys. Rev. A* **77**, 012307 (2008).
- [26] K. Takeda, J. Kamioka, T. Otsuka, J. Yoneda, T. Nakajima, M. R. Delbecq, S. Amaha, G. Allison, T. Kodera, S. Oda, and S. Tarucha, A fault-tolerant addressable spin qubit in a natural silicon quantum dot, *Sci. Adv.* **2**, e1600694 (2016).